Selenium Tethered Copper Phthalocyanine Hierarchical Aggregates as Electrochemical Hydrogen Evolution Catalysts

[a]Indherjith Sakthinathan, [a]Manivannan Mahendran, [b]Karthik Krishnan*, [c]Selvakumar Karuthapandi*

a Electroorganic Division, CSIR-Central Electrochemical Research Institute, Karaikudi, Tamil Nadu-630003, India.

b Corrosion and Material Protection Division, CSIR-Central Electrochemical Research Institute, Karaikudi, Tamil Nadu-630003, India.

c Department of Chemistry, School of Advanced Sciences, VIT-AP University, Amaravati, AP 522237, India.

E-mail: selvakumar.k@vitap.ac.in, karthikk@cecri.res.in

1. Abbreviation

CuPc	Copper Phthalocyanine
CV	Cyclic Voltammetry
DBU	1,8-Diazabicyclo[5.4.0]undec-7-ene
DCM	Dichloromethane
DMF	N,N'-dimethylformamide
ECSA	Electrochemical active surface area
EIS	Electrochemical Impedance Spectroscopy
EPR	Electron Paramagnetic Resonance
FAs	Fibrous Aggregates
GCE	Glassy carbon electrode
HER	Hydrogen Evolution Reaction
LSV	Linear Sweep Voltammetry
MALDI	Matrix-assisted laser desorption/ionization
MeOH	Methanol
MPcs	Metallophthalocyanines
NMR	Nuclear magnetic resonance
n-Oct	n-Octyl
PAs	Particulate aggregates
SEM	Scanning Electron Microscopy
TEM	Transmission Electron Microscopy
TGA	Thermal gravimetric analysis
XPS	X-ray photoelectron spectroscopy

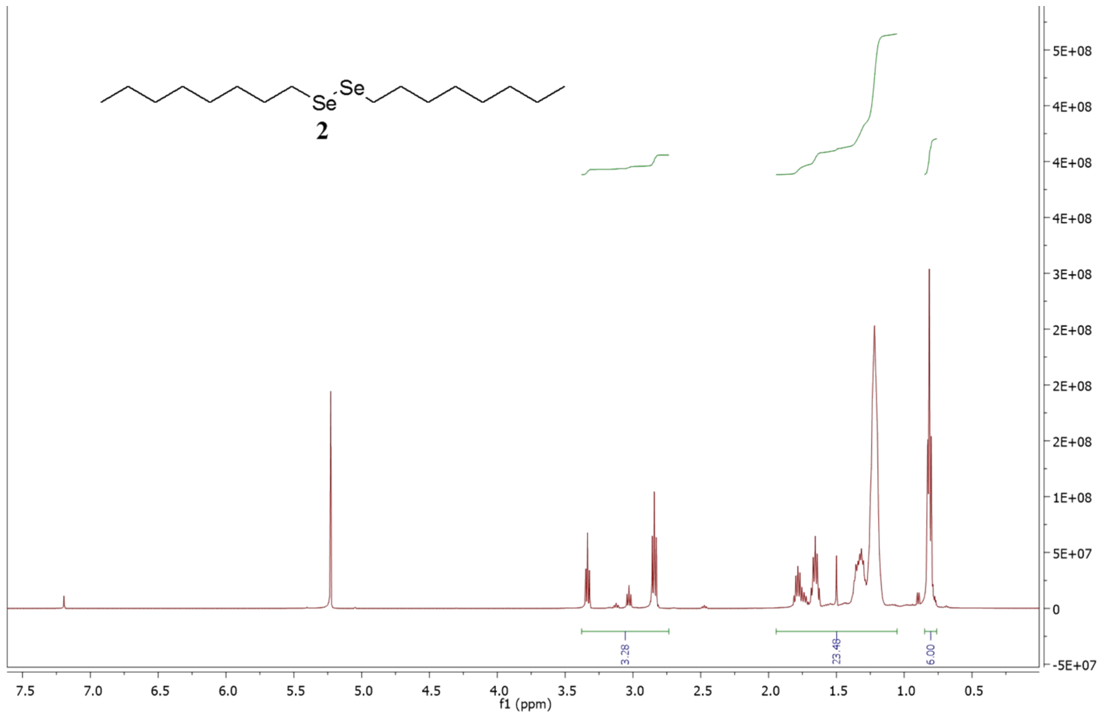

1. N

MR

2

Spectrum

Fig S1. ^{1}H NMR spectra of 1,2-dioctyldiselane.

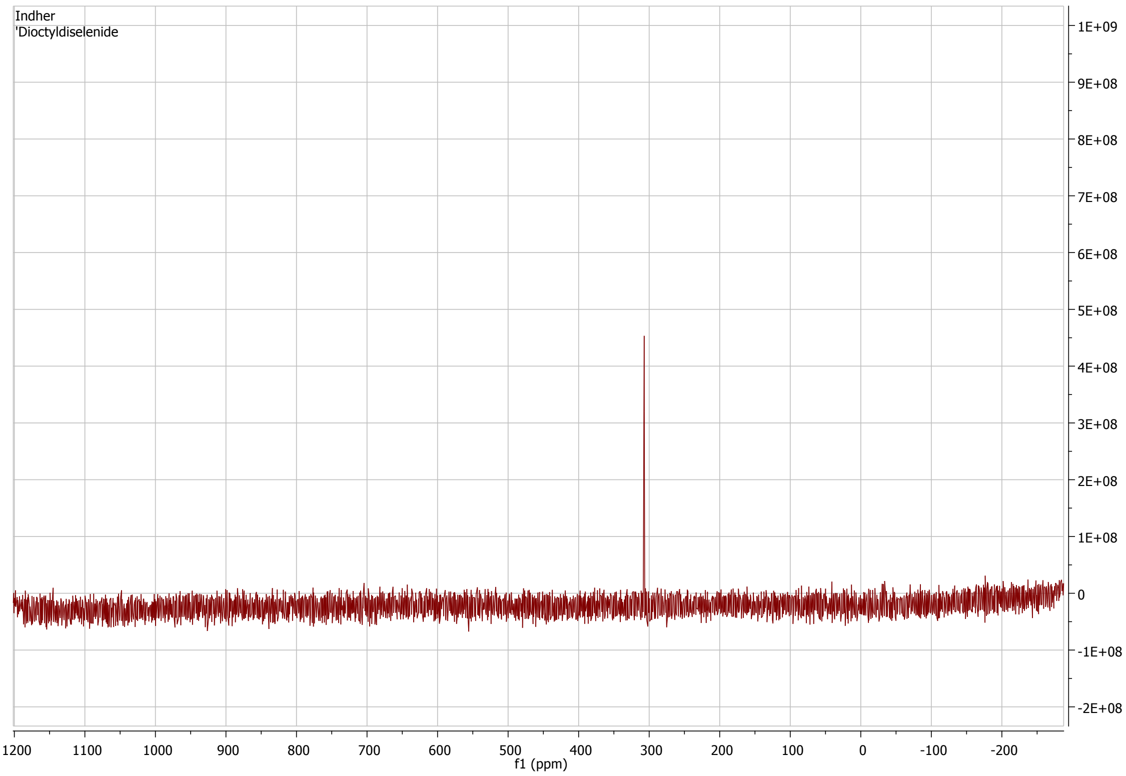

Fig S2. ^{77}Se NMR spectra of 1,2-dioctyldiselane.

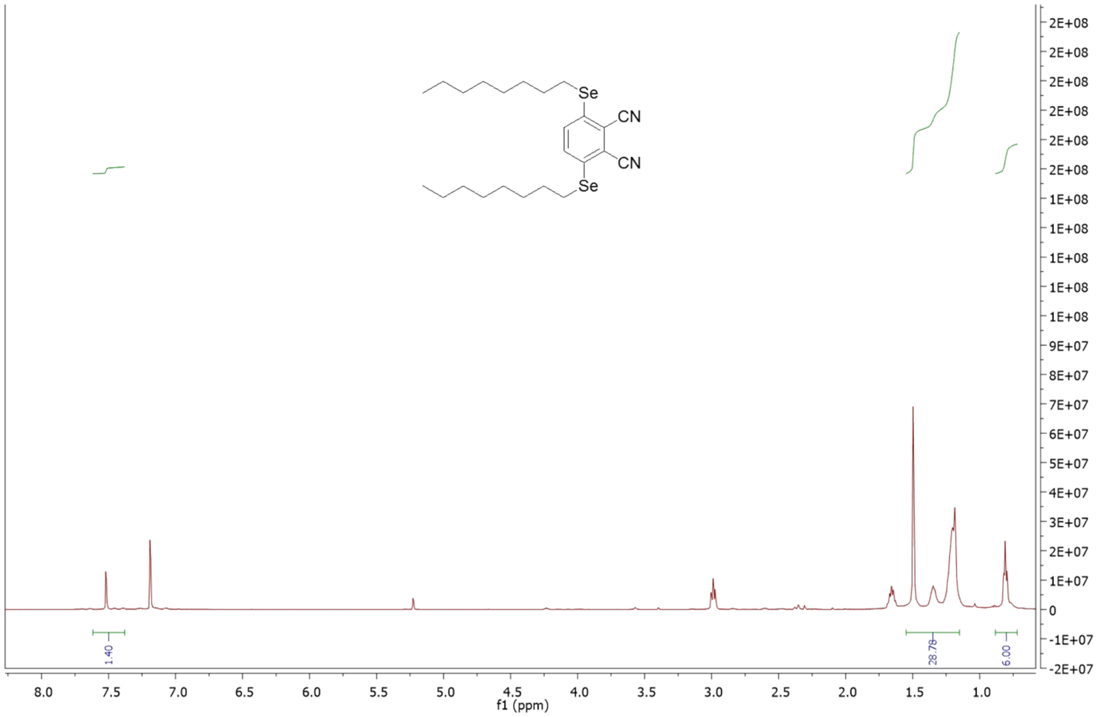

Fig S3. ¹H NMR spectra of 3,6-Bis (n-octylseleno)phthalodinitrile.

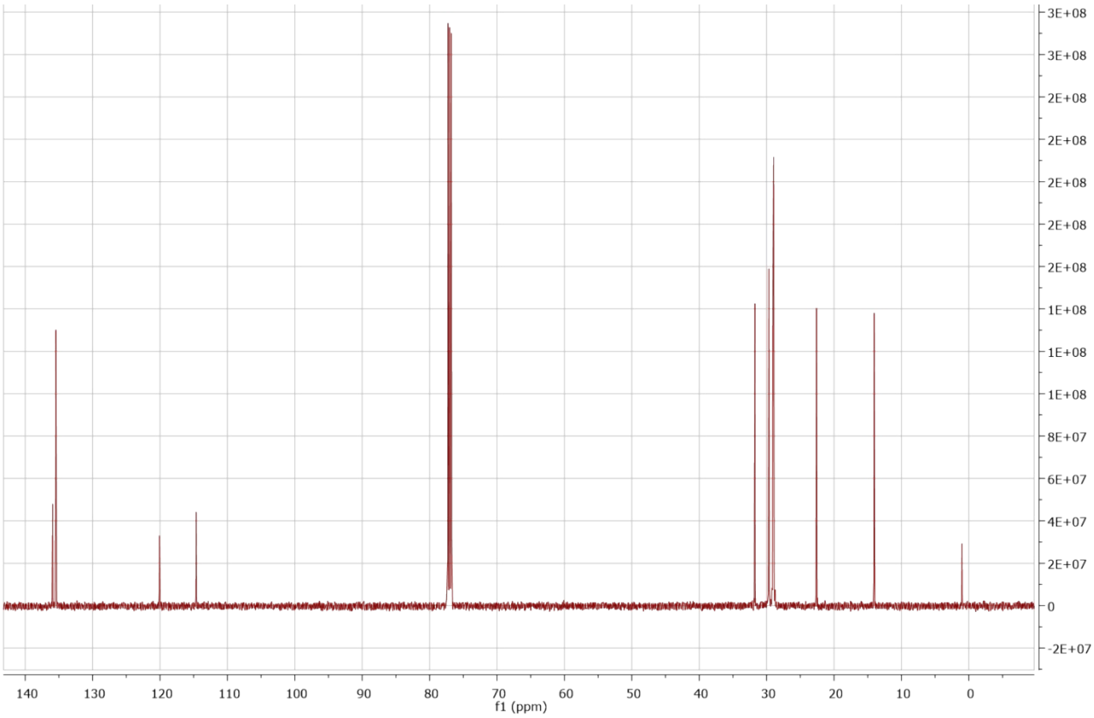

Fig S4. ^{13}C NMR spectra of 3,6-Bis (n-octylseleno)phthalodinitrile

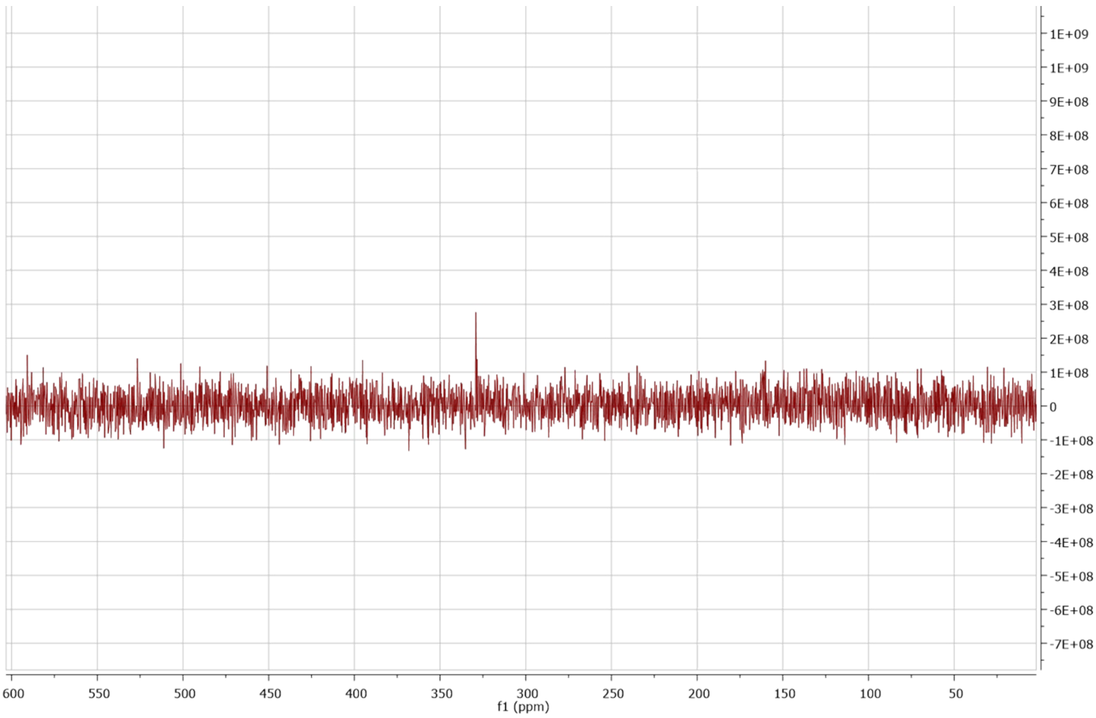

Fig S5. ^{77}Se NMR spectra of 3,6-Bis (n-octylseleno)phthalodinitrile.

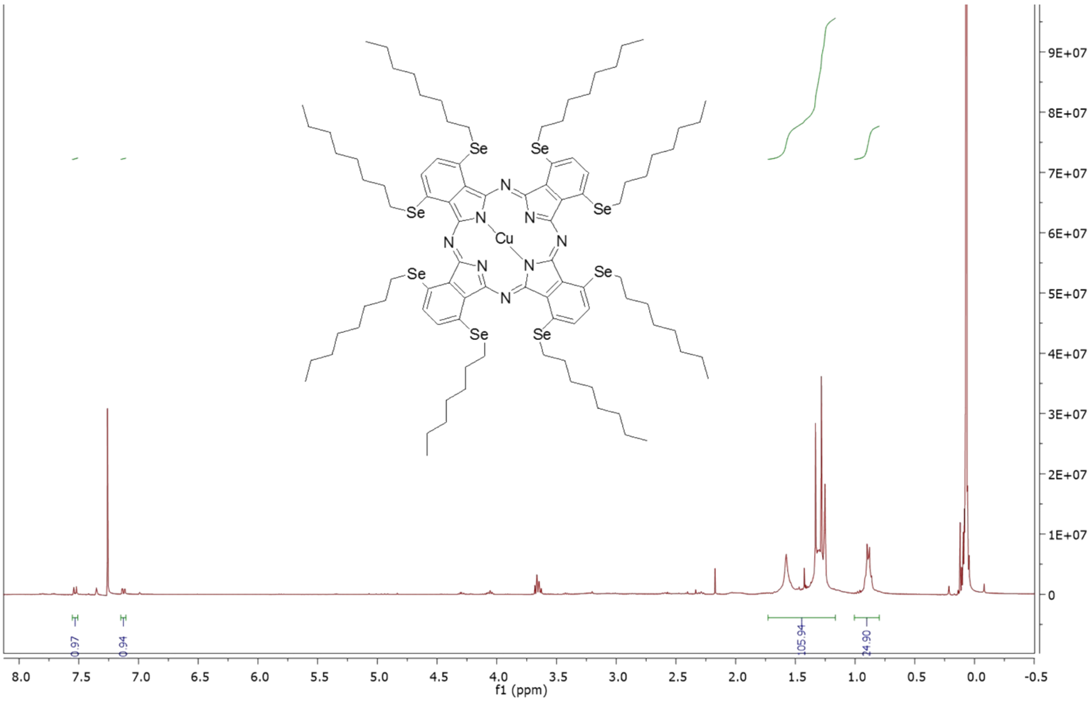

Fig S6. ^{1}H NMR spectra of (n-OctSe)$_8$CuPc

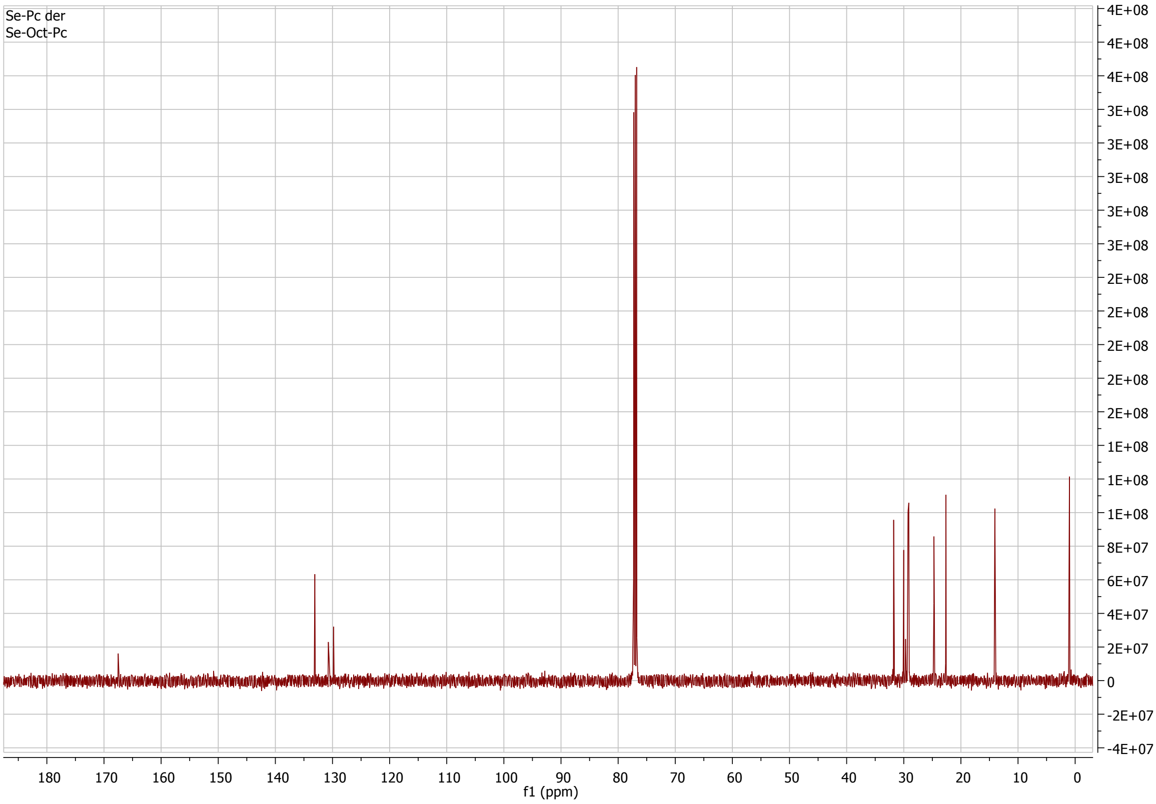

Fig S7. ^{13}C NMR spectra of (n-OctSe)$_8$CuPc

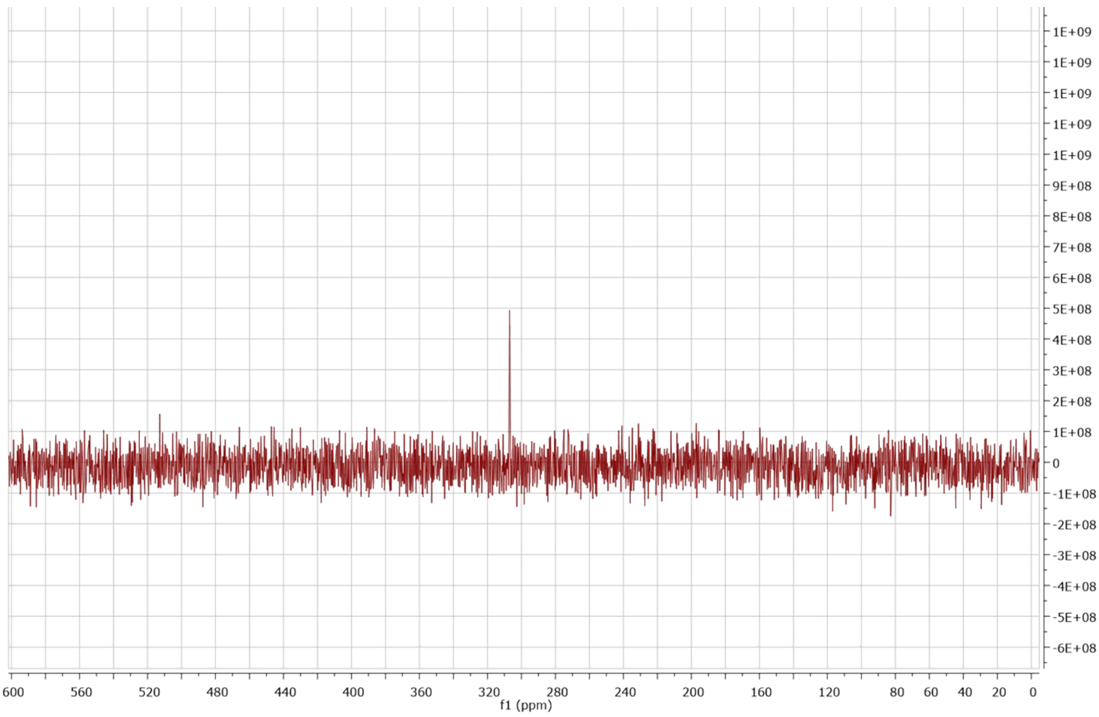

Fig S8. ^{77}Se NMR spectra of (n-OctSe)$_8$CuPc

3. UV-Visible spectrum of (n-OctSe)$_8$CuPc

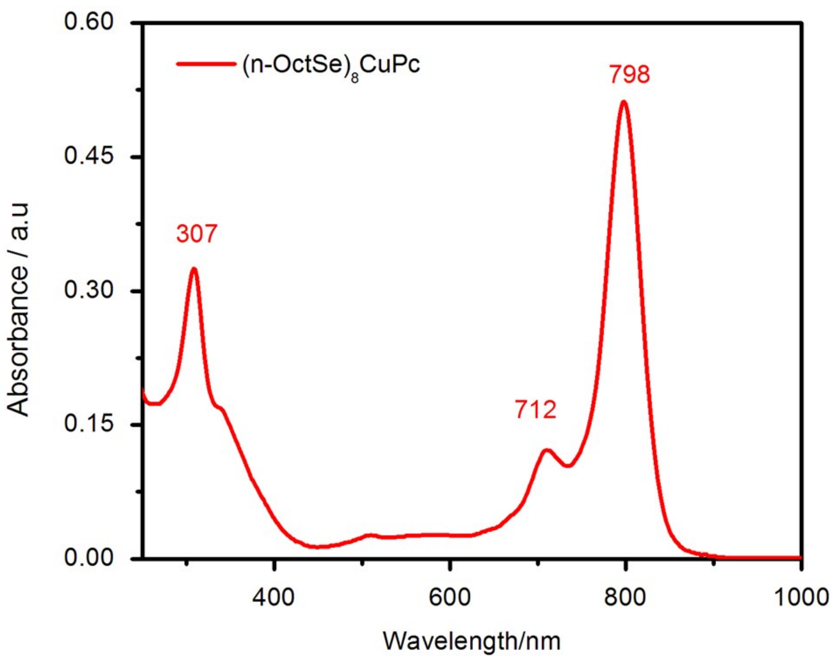

Fig S9. UV-Visible spectrum of (n-OctSe)$_8$CuPc, recorded in dichloromethane.

4. EPR spectrum of (n-OctSe)$_8$CuPc

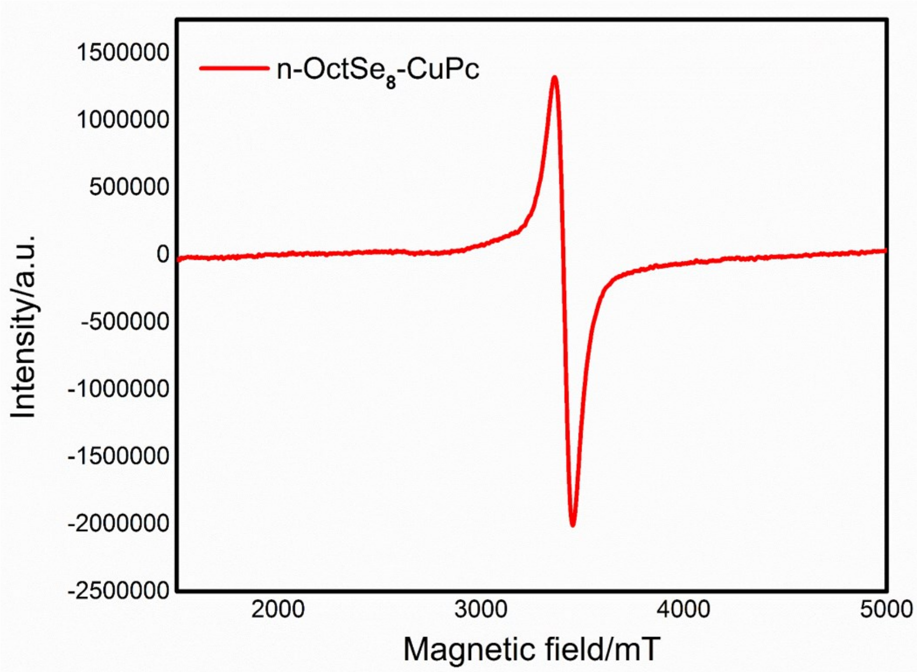

Fig S10. EPR spectrum of (n-OctSe)$_8$-CuPc.

5. Cyclic voltammogram of (n-OctSe)$_8$-CuPc

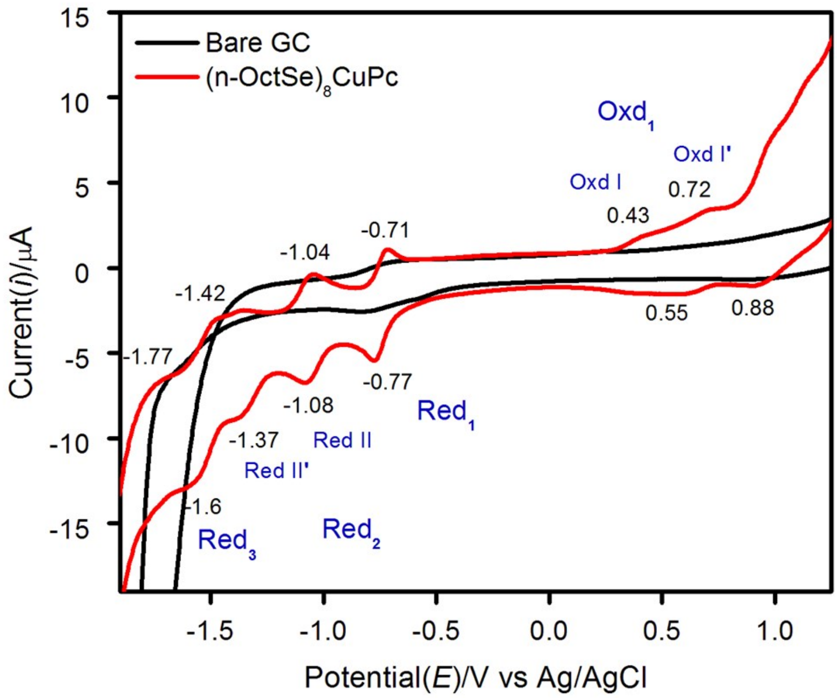

Fig S11. Shows the cyclic voltammograms of (n-OctSe)$_8$-CuPc (1 mM) in CH_2Cl_2 containing 0.1 M of tetrabutylammonium hexafluorophosphate as supporting electrolyte.

6. A general scheme for selenoxide elimination reaction

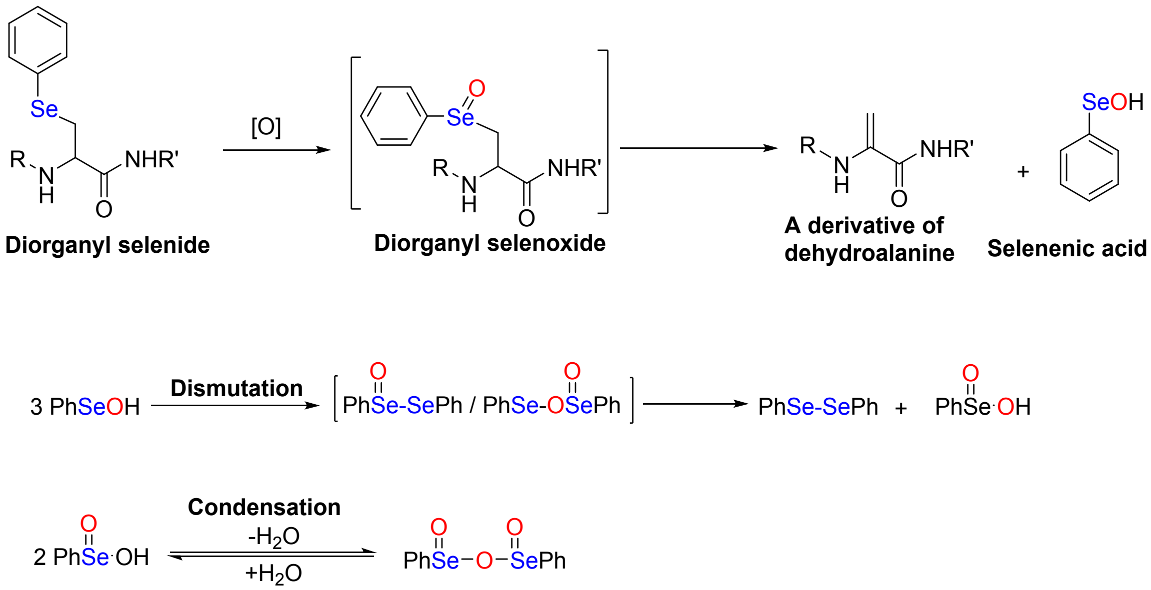

Fig S12. Reaction pathways for selenoxide elimination reaction, and subsequent dismutation-condensation reaction for a general case

7. MALDI Characterization

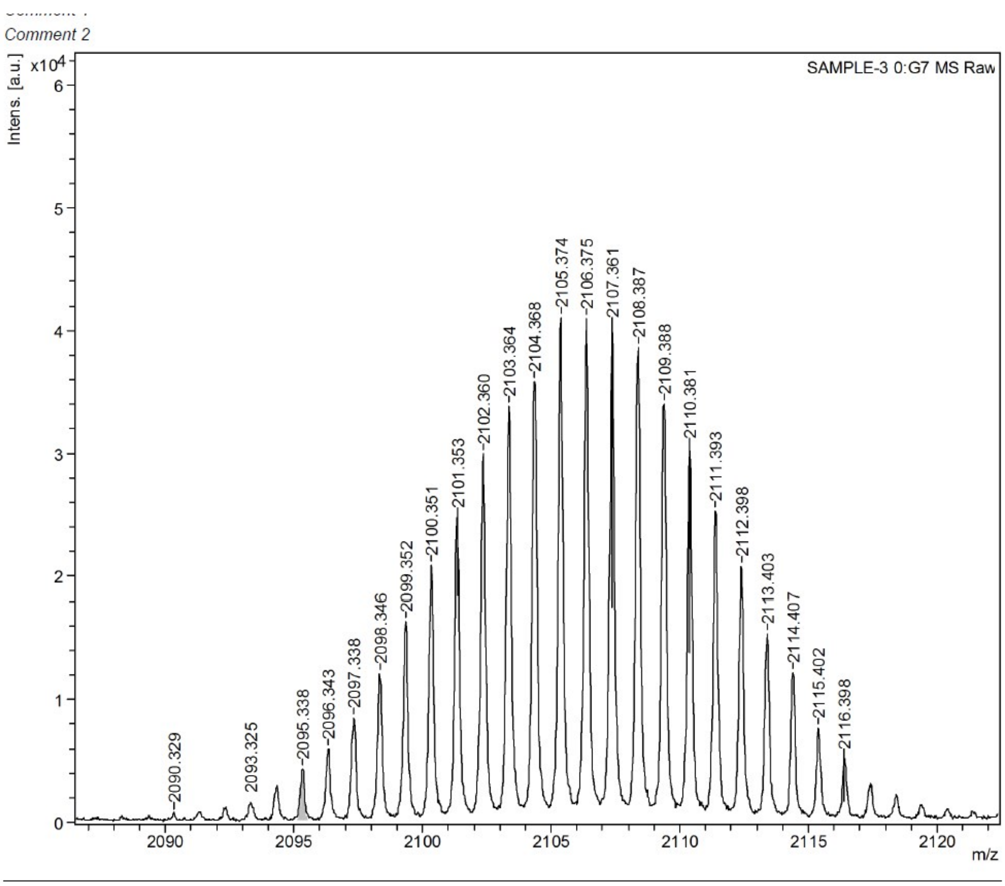

Fig S13. Shows the MALDI mass spectrometry peaks of compound **4**

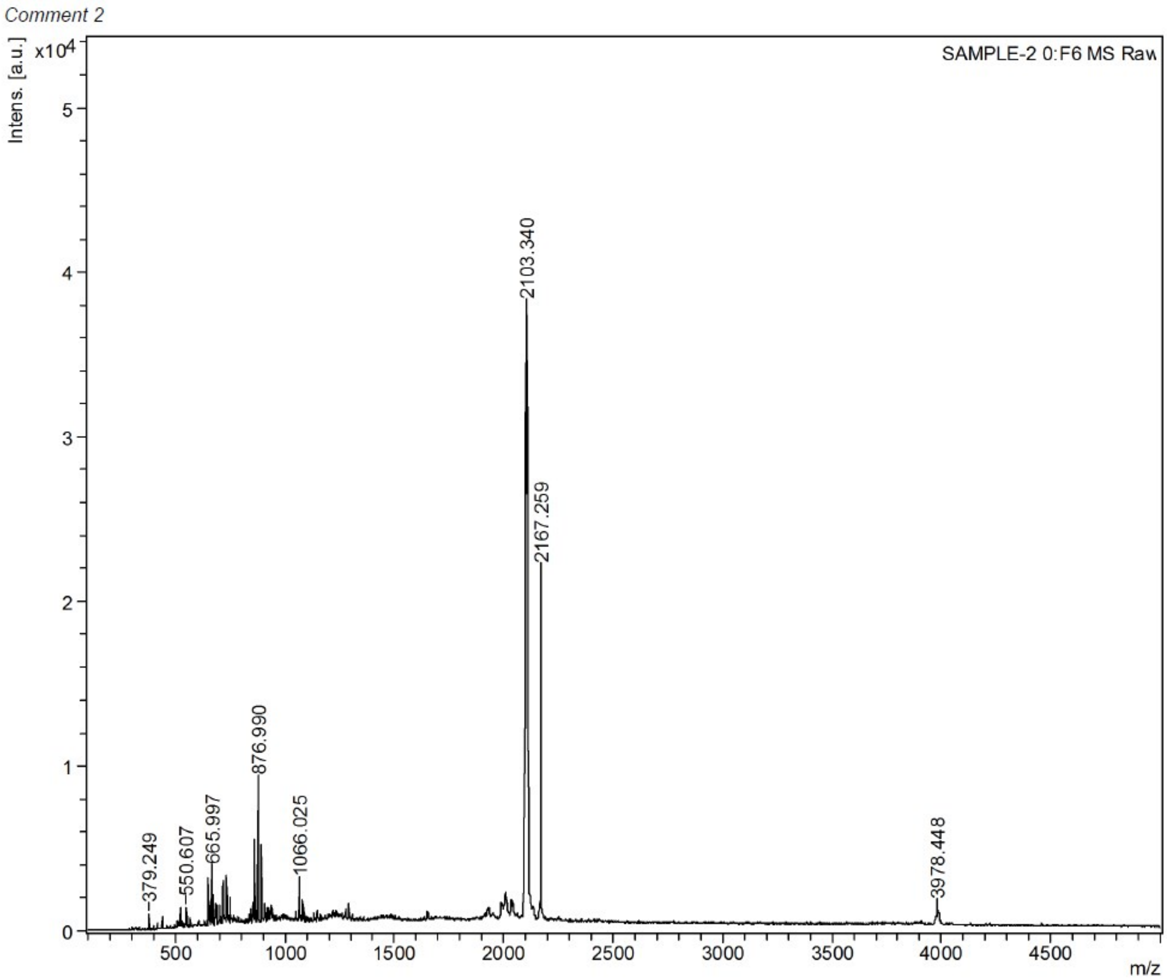

Fig S14. Shows the MALDI mass spectrum of intermediate species observed from the extract of FAs. It shows the peak corresponding to compound **4** (@m/z, 2103.340), **7** (@m/z, 2167.259), and **8** (@m/z, 3978.44. The expansion and the peaks corresponding to species **7** and **8** are provided below in figure **S15** and **S16** respectively.

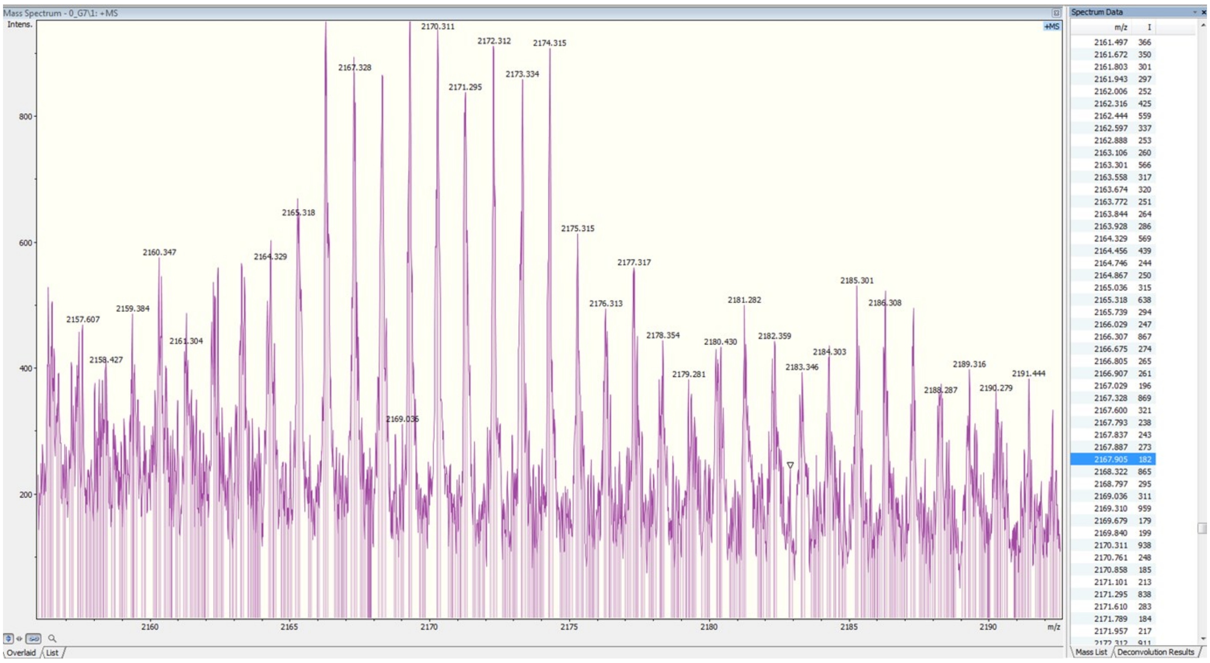

Fig S15. Expansion of peak observed for selenoxide **7**

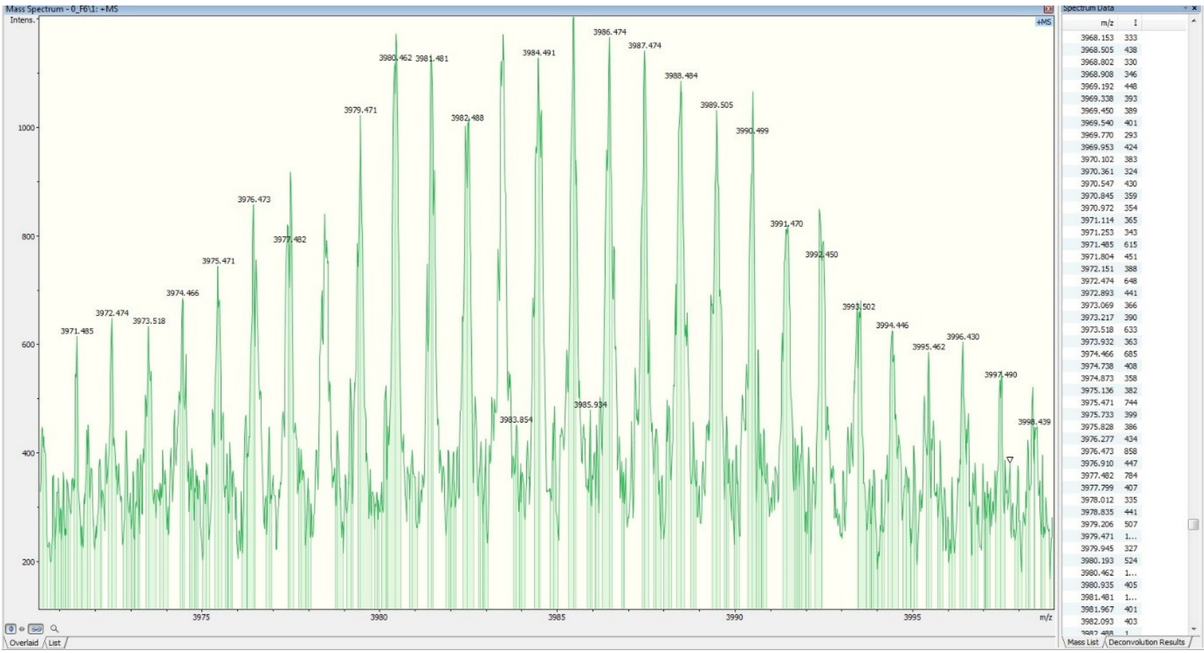

Fig S16. Expansion of peak observed for diselenide **8**

8. X-Ray Photoelectron Spectroscopic (XPS) data

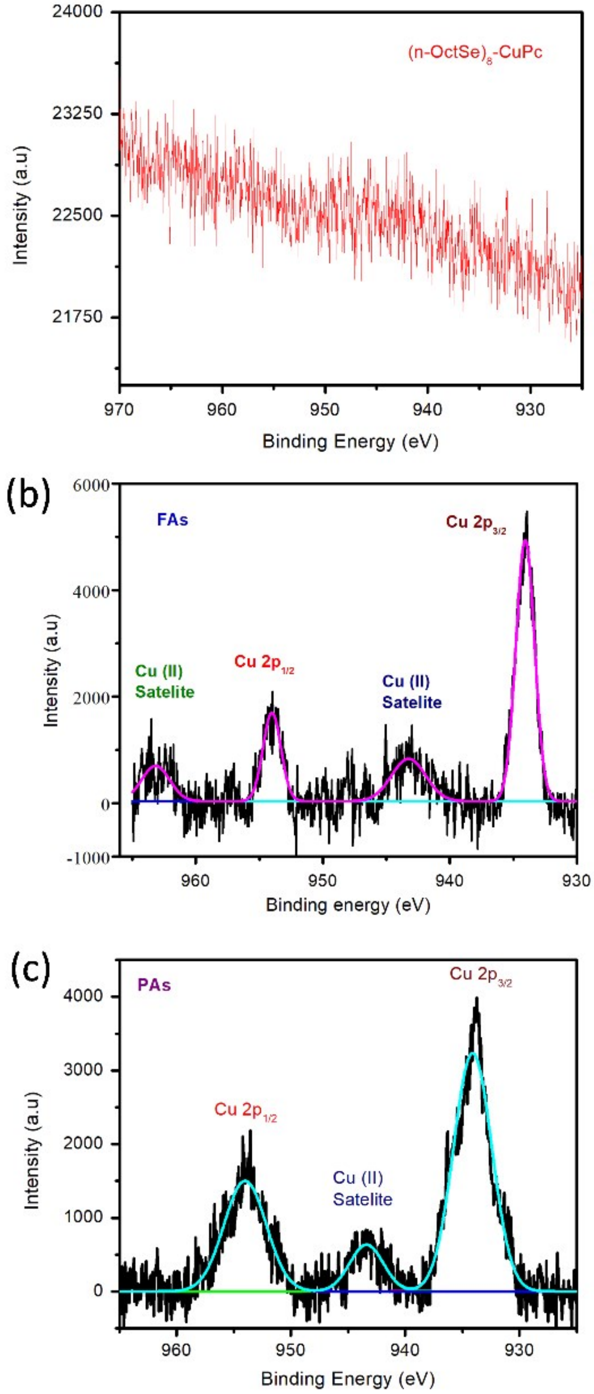

Fig S17. Shows the XPS of copper present in the a) $(nOctSe)_8$-CuPc, b) FAs, and c) PAs.

9. FTIR spectrum FAs and PAs

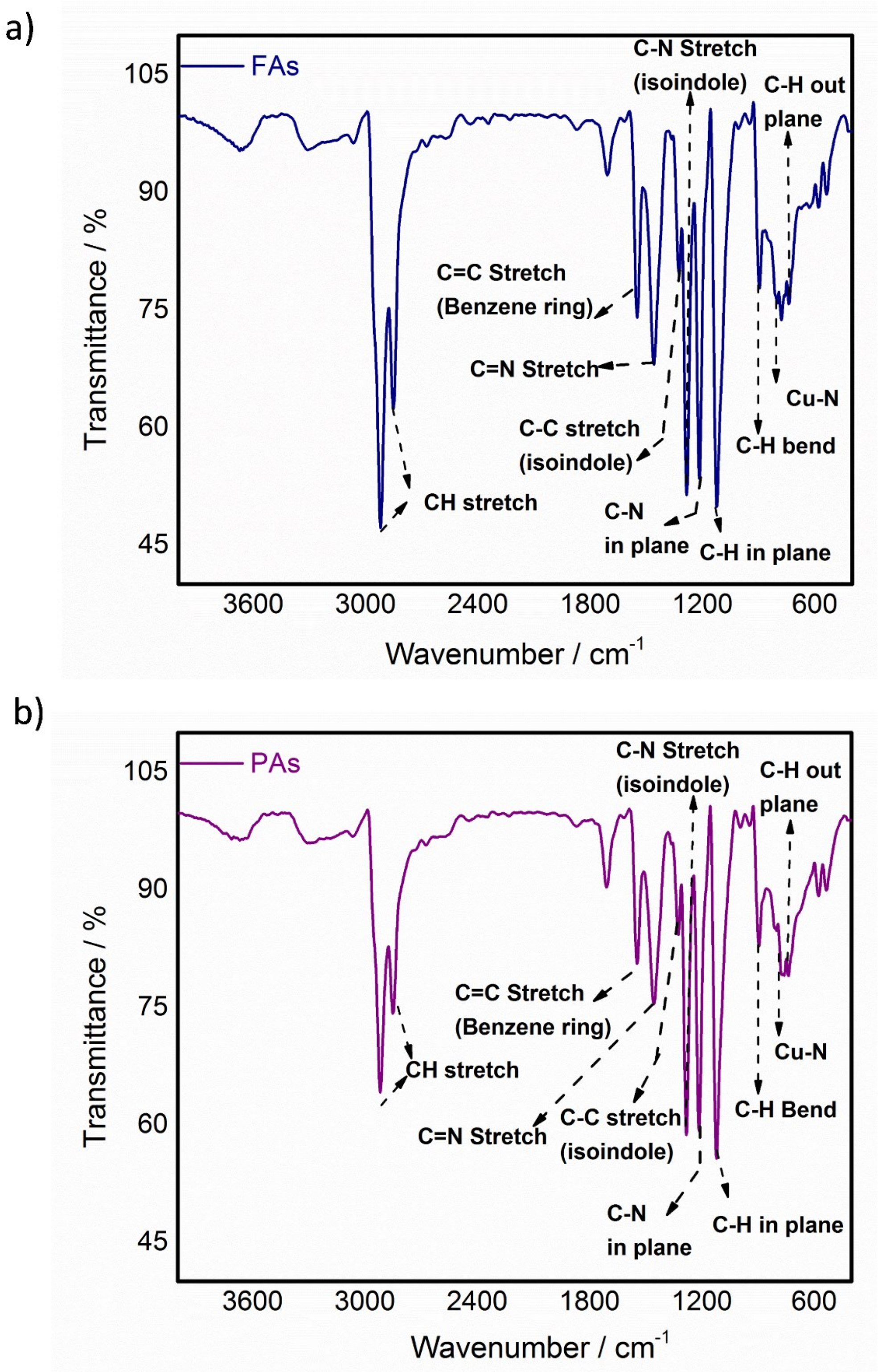

Fig S18. Shows the FTIR spectrum of a) FAs, and b) PAs

10. Electrochemically active surface area (EASA) measurements

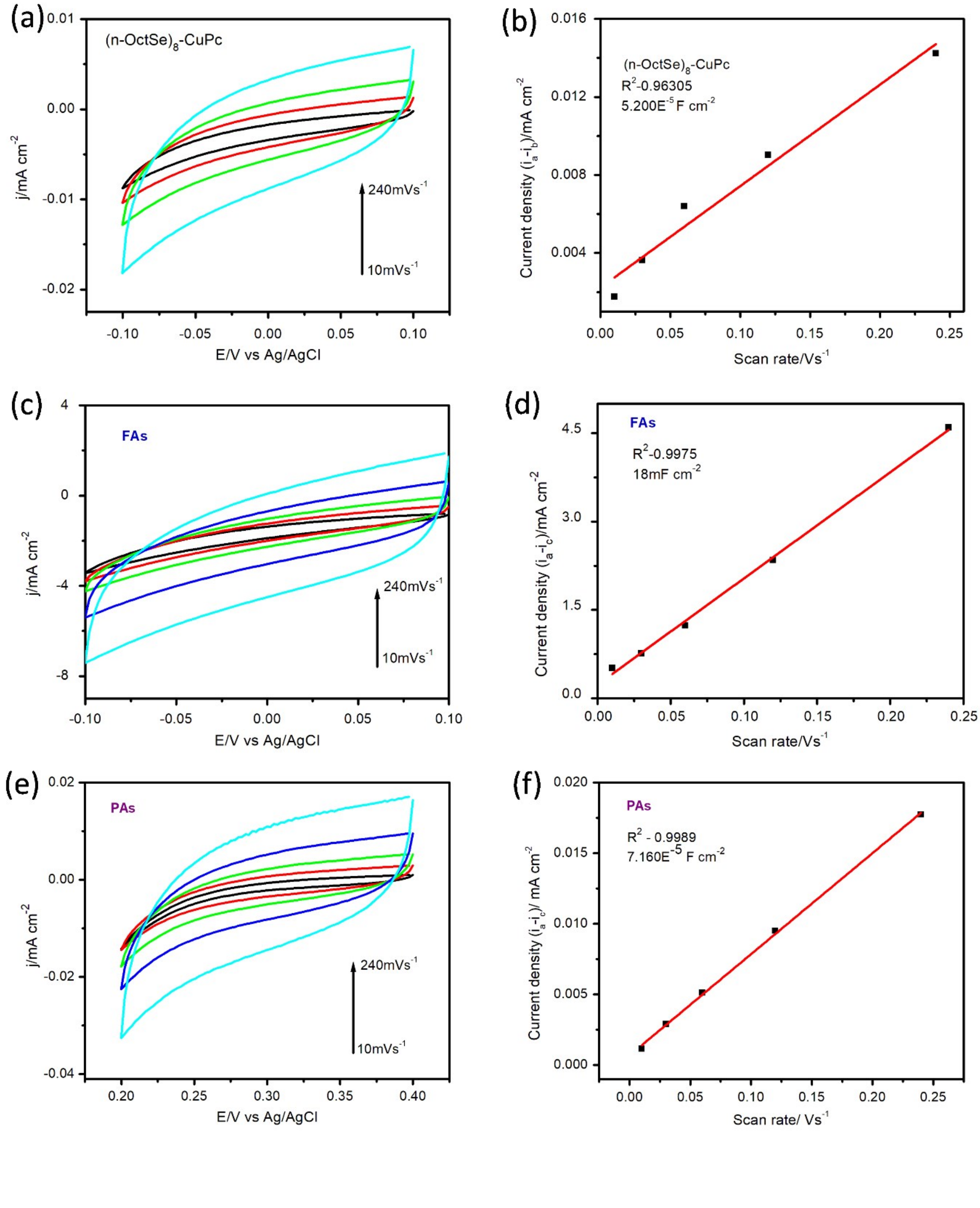

Fig S19. CV, current density Vs Potential (E) plots; a, c, e, correspond to (n-OctSe)$_8$-CuPc, FAs, and PAs respectively. Figure b, d, f are corresponding current density Vs scan rate plot. The CV was recorded in 0.5M H_2SO_4 solution with Ag/AgCl as reference electrode.

11. Cycling stability of FAs and PAs

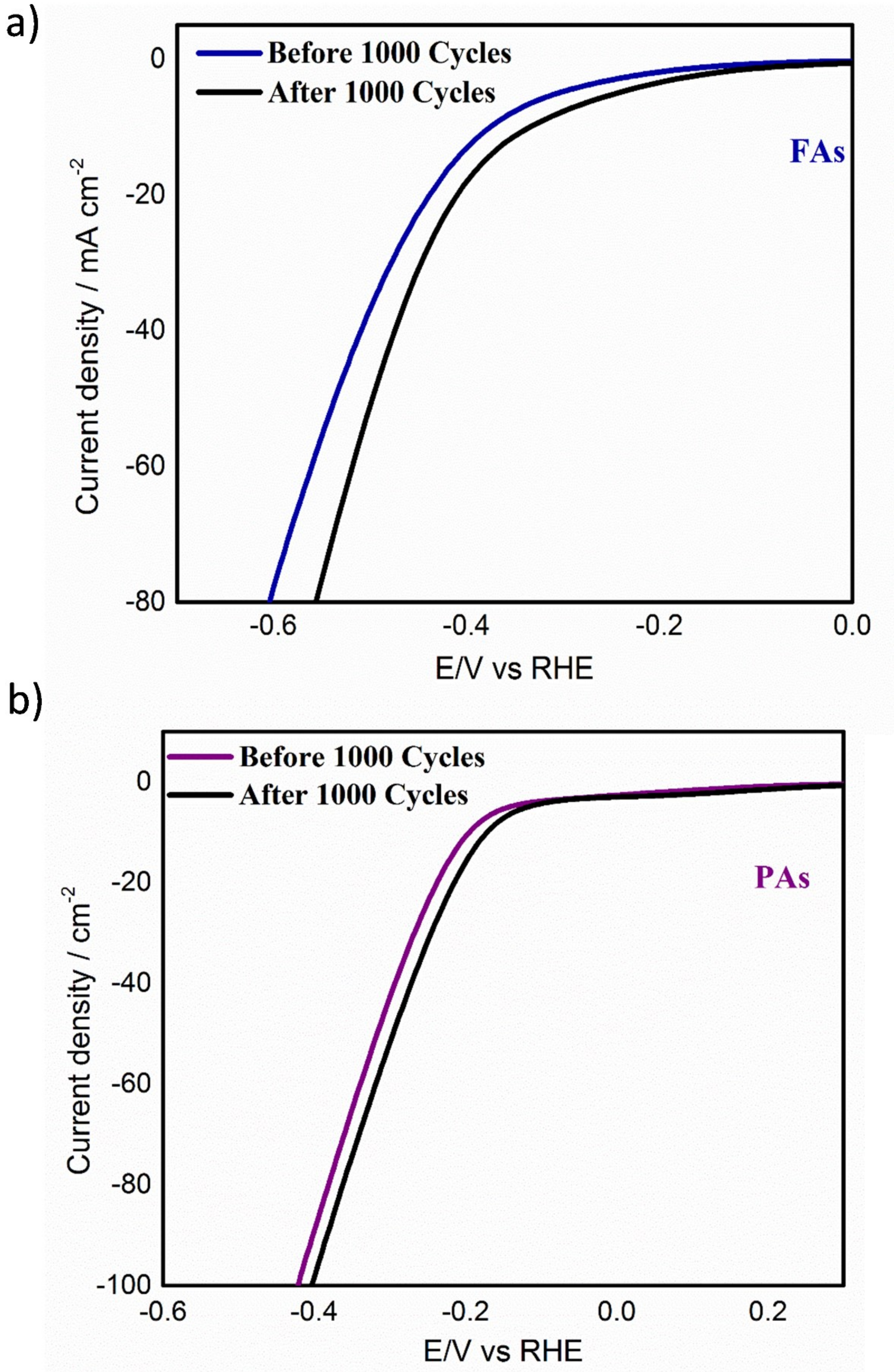

Fig S20. Shows polarization graph of cycle 1 and cycle 1000 for a) FAs and b) PAs

12. Post-HER TEM imaging

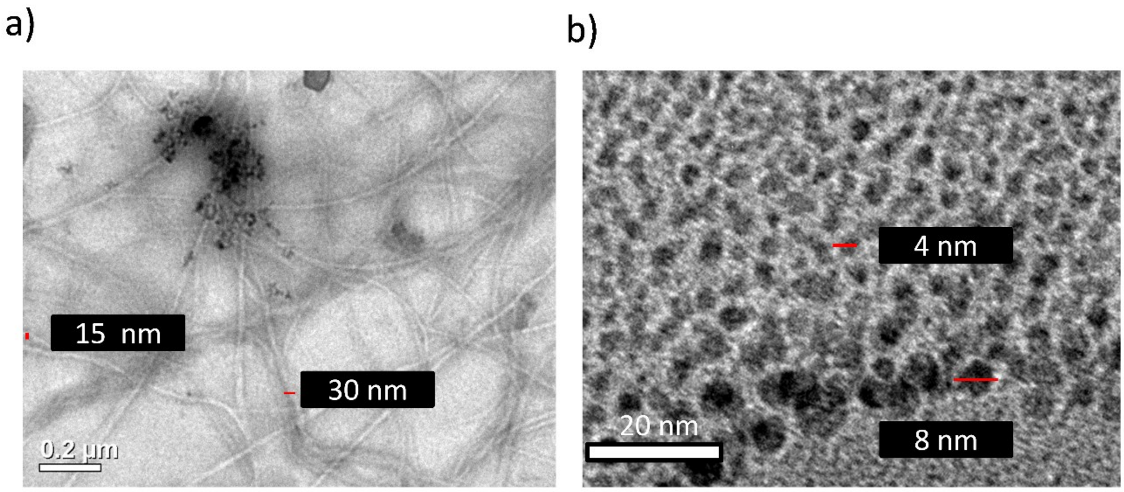

Fig. S21. Shows the TEM images taken after chronoampherometric HER; a) FAs, b) PAs

13. FTIR Spectrum of PAs before and after catalysis

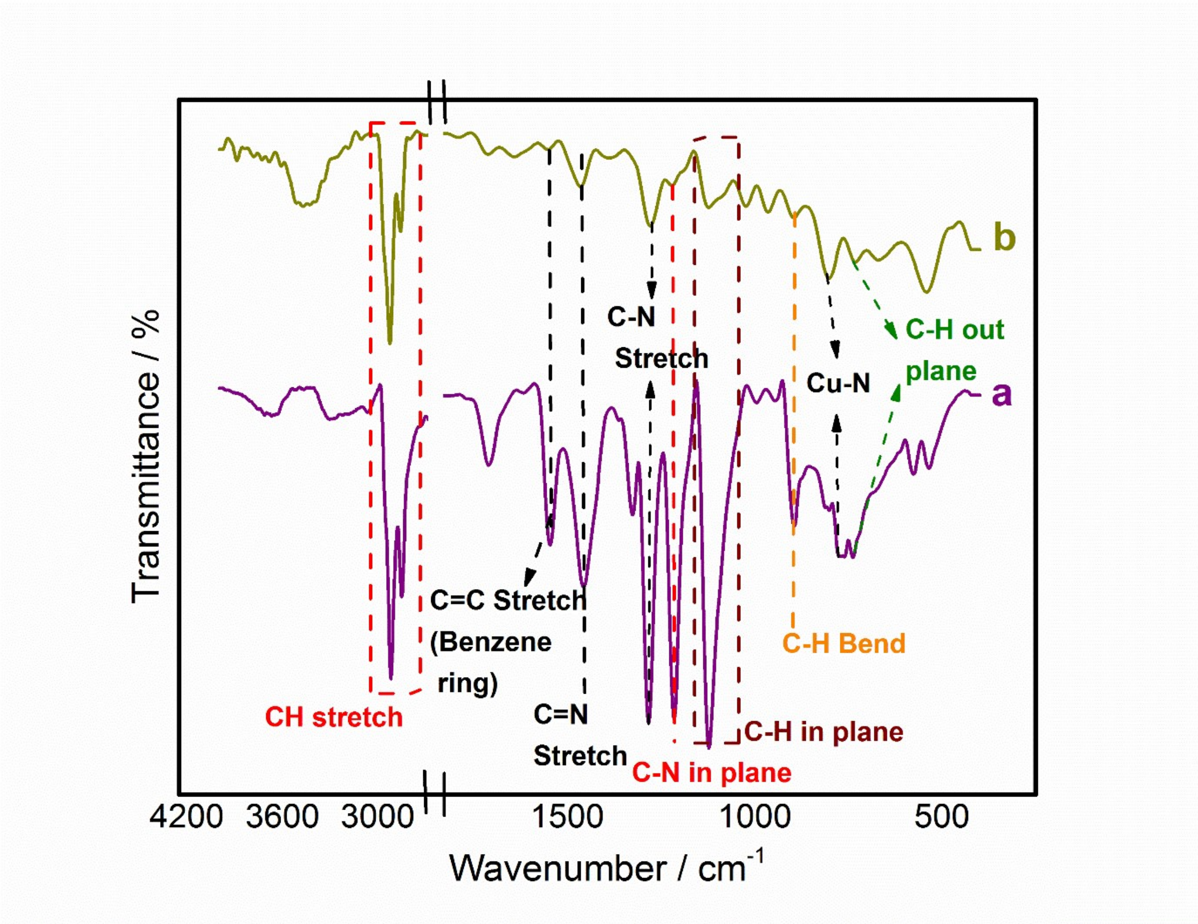

Fig. S22. Shows the FTIR spectrum of PAs a) before catalysis b) after catalysis

14. HER overpotential comparison

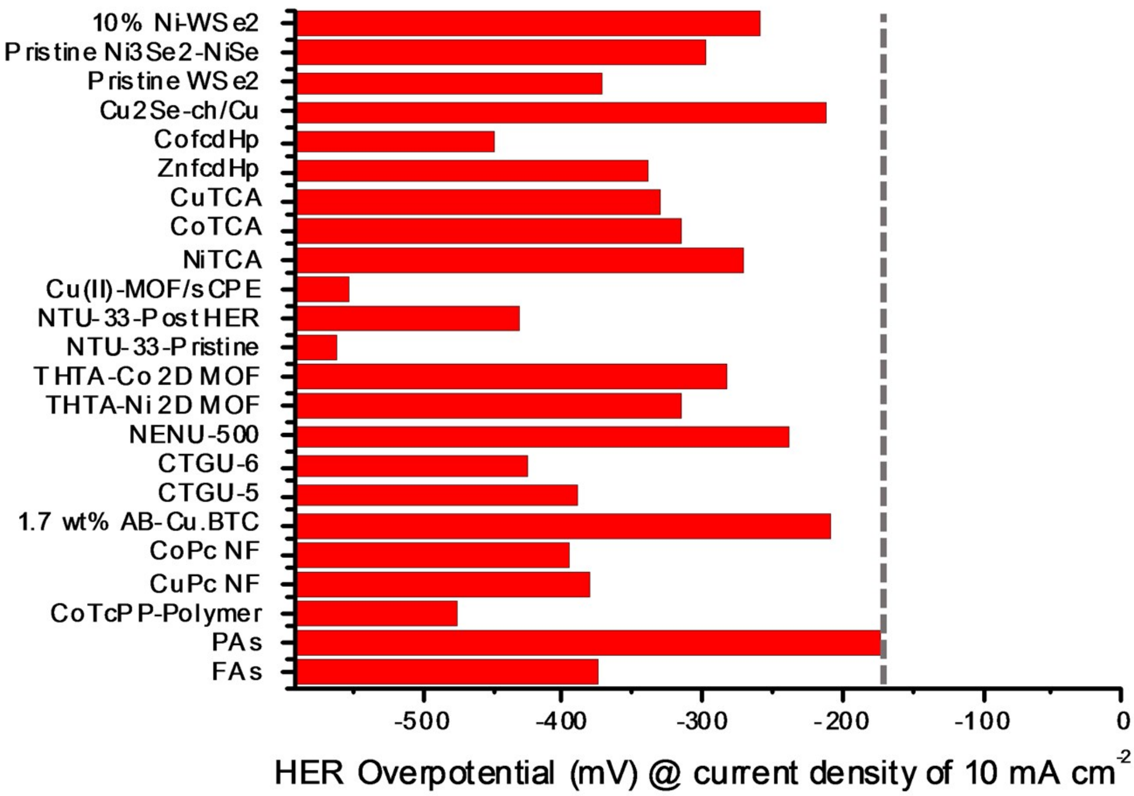

Fig S23. Histogram plot comparing HER overpotential (mV (x-axis)) of PAs with other coordination polymers and MOFs reported in the literature (Table S2).

15. Table S1 and Table S2

Table S1. Cyclic voltammetric data for compound **4**

Compound	Redox Waves	$E_{1/2}$(V)	E_p(mV)	$I_{p,a}/I_{p,c}$
	Red_1	-0.74	60	0.23
(n-OctSe)$_8$-CuPc	Red_2 (Red II (Red II'))	-1.06 (-1.40)	40 (50)	0.57 (0.32)
	Red_3	-1.69	170	0.52
	Oxd_1 (Oxd I (Oxd I'))	0.49 (0.80)	120 (160)	1.21 (2.6)

[a] $E_{1/2}$ $(E_{pa}+E_{pc})/2$) were recorded at 100 mV/s scan rate
[b] $\Delta E_p = E_{pa} - E_{pc}$
[c] $I_{p,a}/I_{p,c}$ for reduction, $I_{p,c}/I_{p,a}$ for oxidation processes.

Table S2; Comparison of HER activity parameters with literature data

Catalyst	η (mV) @ 10mAcm^{-2}	Tafel slope [mV/dec]	Electrolytes	Ref
FAs	-375	252	0.5 M H_2SO_4	This work
PAs	-172	180	0.5 M H_2SO_4	This work
CoTcPP-Polymer	-475	197	0.5 M H_2SO_4	[1]
FCoP@CNT	-576[a]	126	0.5M H_2SO_4	[2]
CuPc NF	-380	121	0.5M H_2SO_4	[3]
CoPc NF	-395	108	0.5M H_2SO_4	[3]
Cu-BTC MOF	-369[b]	135	0.5M H_2SO_4	[4]
1.7 wt% AB-Cu.BTC	-208	80	0.5M H_2SO_4	[5]
CTGU-5	-388	125	0.5M H_2SO_4	[6]
CTGU-6	-425	176	0.5M. H_2SO_4	[6]
NENU-500	-237	96	0.5M H_2SO_4	[7]
THTA-Ni 2D MOF	-315	76	0.5M H_2SO_4	[8]
THTA-Co 2D MOF	-283	71	0.5M H_2SO_4	[8]
NTU-33-Pristine	-560	158	0.5M H_2SO_4	[9]
NTU-33-Post HER	-430	129	0.5 M H_2SO_4	[9]

Cu(II)-MOF/sCPE	-552	62	1.0 M H_2SO_4	[10]
NiTCA	-270	89	0.5M H_2SO_4	[11]
CoTCA	-315	96	0.5M H_2SO_4	[11]
CuTCA	-330	100	0.5M H_2SO_4	[11]
ZnfcdHp	-340	110	0.5 M H_2SO_4	[12]
CofcdHp	-450	120	0.5 M H_2SO_4	[12]
Cu_2Se-ch/Cu	-212	32	0.5 M H_2SO_4	[13]
Pristine WSe_2	-372	105	0.5 M H_2SO_4	[14]
Pristine Ni_3Se_2–NiSe	-298	71	0.5 M H_2SO_4	[14]
10% Ni–WSe_2	-259	86	0.5 M H_2SO_4	[14]

[a]to reach 1mAcm^{-2}, [b]to reach 30mAcm^{-2}

16. References

1 Y. Wu, J. M. Veleta, D. Tang, A. D. Price, C. E. Botez and D. Villagrán, *Dalt. Trans.*, 2018, **47**, 8801–8806.

2 G. Xu, H. Lei, G. Zhou, C. Zhang, L. Xie, W. Zhang and R. Cao, *Chem. Commun*, 2019, **55**, 12647–12650.

3 K. P. Madhuri and N. S. John, *ChemistrySelect*, 2019, **4**, 7292–7299.

4 M. Jahan, Z. Liu and K. P. Loh, *Adv. Funct. Mater.*, 2013, **23**, 5363–5372.

5 X. Wang, W. Zhou, Y. Wu, J. Tian, X. Wang, D. Huang, J. Zhao and D. Li, *J. Alloys Compd.*, 2018, **753**, 228–233.

6 Y. Wu, W. Zhou, J. Zhao, W. Dong, Y. Lan, D. Li, C. Sun and X. Bu, *Angew. Chemie - Int. Ed.*, 2017, **56**, 13001–13005.

7 J. Qin, D. Du, W. Guan, X. Bo, Y. Li, L. Guo, Z. Su, Y. Wang, Y. Lan and H. Zhou, *J. Am. Chem. Soc*, 2015, **137**, 7169–7177.

8 R. Dong, Z. Zheng, D. C. Tranca, J. Zhang, N. Chandrasekhar, S. Liu, X. Zhuang, G. Seifert and X. Feng, *Chem. - A Eur. J.*, 2017, **23**, 2255–2260.

9 B. Zhou, J. Zheng, J. Duan, C. Hou, Y. Wang, W. Jin and Q. Xu, *ACS Appl. Mater. Interfaces*, 2019, **11**, 21086–21093.

10 D. He, J. Liu, Y. Wang, F. Li, B. Li and J. He, *Electrochim. Acta*, 2019, **308**, 285–294.

11 S. R. Vishwanath and S. Kandaiah, *J. Mater. Chem. A*, 2017, **5**, 2052–2065.

12 R. Shekurov, V. V.Khrizanforova, L. Gilmanova, M. N. Khrizanforov, V. Miluykov, O. Kataeva, Z. Yamaleeva, T. Burganov, T. Gerasimova, A. Khamatgalimov, S. Katsyuba, V. Kovalenko, Y. Krupskaya, V. Kataev, B. Büchner, V. Bon, I. Senkovska, S. Kaskelf, A. Gubaidullina, O. G.Sinyashin and Y. H.Budnikova, *Dalt. Trans.*, 2019, **48**, 3601–3609.

13 S. Anantharaj, T. S. Amarnath, E. Subhashini, S. Chatterjee, K. C. Swaathini, K. Karthick and S. Kundu, *ACS Catal.*, 2018, **8**, 5686–5697.

14 S. R. Kadam, A. N. Enyashin, L. Houben, R. Bar-Ziv and M. Bar-sadan, *J. Mater. Chem. A*, 2020, **8**, 1403–1416.